
REAL-TIME HIGH RESOLUTION THZ IMAGING WITH A FIBER COUPLED PHOTO CONDUCTIVE ANTENNA AND AN UNCOOLED MICROBOLOMETER CAMERA

A PREPRINT

✉ Peter Zolliker*, ✉ Elena Mavrona, ✉ Erwin Hack

Transport at Nanoscale Interfaces Laboratory
Empa, Swiss Federal Laboratories for Materials Science and Technology
Überlandstrasse 129, 8600 Dübendorf, Switzerland

Mostafa Shalaby and Elisa Söllinger

Swiss Terahertz Research-Zurich, Swiss Terahertz GmbH
Technopark, 8005 Zurich, Switzerland and Park Innovaare, 5234 Villigen, Switzerland

April 9, 2021

ABSTRACT

We present a real-time THz imaging method using a commercial fiber coupled photo conductive antenna as the THz source and an uncooled microbolometer camera for detection. Compared to other THz imaging setups, this concept is very adaptable due to its compact and uncooled radiation source, whose fiber coupling allows for a flexible placement. Using a camera with high sensitivity renders real-time imaging possible. As a proof-of-concept, the beam shape of a THz Time Domain Spectrometer was measured. We also demonstrate the potential for practical applications in transmission geometry, covering material science and security tasks. The results suggest that hidden items, complex structures and moisture contents of (biological) materials can be resolved. We discuss the limits of the current setup, possible improvements, potential (industrial) applications and outline the feasibility of imaging in reflection geometry or extending it to multi-spectral imaging using band pass filters.

Keywords THz imaging; real-time; photo conductive antenna; microbolometer camera; THz-TDS

1 Introduction

In material science, as well as in industrial and security applications, non-destructive testing of samples is an important prerequisite. Non-ionizing THz radiation can be an option, since it can deliver sub-millimeter resolution. Additionally, many materials have high transmissivity in this frequency range. A broad range of materials like plastics [1, 2, 3, 4], ceramics [5, 6], illicit drugs [7, 8, 9], explosives [8, 9, 10], wood [11, 12, 13], paper [14, 15], leaves [10, 16] and blood [17, 18] have been successfully studied with THz radiation. Also, a large number of security applications based on (sub-)THz radiation [8] have been proposed and some are commercially available [8, 19]. Despite the immense potential, application of THz outside research is currently far from being common. In theory, a THz transmission imaging setup can be made out of a single line source, a collimating lens and a pixel array camera. This simplistic setup is a promising candidate for industrial and security applications. However, the achievable resolution and image quality, respectively, are limited by the irradiation wavelength, the numerical aperture NA of all optical components, as well as by the camera properties (pixel size, sensitivity, etc.). To circumvent especially the limitations of the optical components, lens-less imaging [20, 21] can be an option.

*Correspondence; peter.zolliker@empa.ch

To date, the most commonly used sources in the frequency range between 0.2 THz and 4 THz are far infrared (FIR) gas lasers, quantum cascade lasers (QCLs) and photo-conductive antennas (PCAs).

The FIR gas lasers [22] are based on a high power, mid-infrared CO₂-laser pumping a THz cavity. Their THz emission can be continuous-wave (cw), with the output power exceeding 150 mW at 2.52 THz [21]. The output wavelength depends on the gas in the THz resonator. However, cw lasers are only emitting a single line and the stable operation can be challenging. Recently, the relatively compact THz QCLs started performing without cryostat, operating with a thermoelectric cooler [23] and at temperatures up to 250 K [24]. In frequency combs operation, the bandwidth has been higher than an octave [25], but still it is limited to 1 THz – 6 THz [26]. Recently, the reported peak output power reached 2 W (58 K, 3.3 THz, single mode) [27]. Despite the promising progress, more research is required to achieve room temperature operation, larger bandwidth and higher power.

PCAs combine many advantages of the above mentioned sources: They are compact, well established broadband sources with bandwidth up to 6 THz and 90 dB dynamic range [28]. Their performance is limited by the near-infrared (NIR) pump pulse, carrier lifetime and the chosen detector. The majority of commercially available THz Time Domain Spectrometer (THz-TDS) use a PCA combined with off-axis parabolic mirrors (OAPMs) as a basis. Application of the compact and robust THz-TDS quickly spread from the first reported use case of water vapor absorption characterization [29] into other research disciplines, even including (art) conservation [30, 31, 32] and archaeology [33, 34, 32, 6]. So far, for THz-TDS imaging only prototypes of multipixel detectors [35] are reported; image acquisition requires a sequential scanning of the sample which cannot provide data in real-time. Nevertheless, scanning THz-TDS paved the way for adaption of THz imaging in industrial applications, e. g. lacquer thickness determination [36, 4]. Due to PCAs being widely available, THz imaging with them is very attractive. For example, Stantchev et al. used a PCA for real-time single pixel imaging [37]. Their method to modulate the THz beam via a digital micromirror device retains the time domain capabilities of the THz-TDS, whilst still achieving a resolution of 32×32 pixels at 6 frames-per-second (fps). Per contra, their approach requires elaborate equipment, whereas we propose a method based on a simple transmission setup, using a PCA as source and exploiting the recent improvements of microbolometer cameras. Our approach can deliver much higher resolution and is more suitable for in-field (industrial) applications, but sacrifices the spectral information.

In this paper, we give a short overview of the method, the camera properties, the setups and describe the data processing. We recorded a THz beam shape in real-time and determined the spatial resolution with a Siemens star. The suitability of the method for practical applications was demonstrated by imaging a key concealed in a paper envelope, the qualitative resolution of different water contents in leaves and imaging of annual rings in wood. Finally, we discuss the limitations and possible improvements of the setup as well as suggest practical applications and future extensions.

2 Setups and Methods

2.1 Camera and lens properties

For the experiments, a Swiss Terahertz RIGI camera and THz lens were used. Their specifications are found in table 1 and 2, respectively.

Camera	Swiss Terahertz RIGI S2x
Type	uncooled THz microbolometer
Operation range	16 – 3000 μm (0.1 – 18 THz)
Pixel size (μm)	25
Number of pixels	160×120
Detector size (L \times H, mm^2)	4×3
NEP	$< 1.5 \text{ pW @ } 4.6 \text{ THz}$
ADC (bit)	14
Frame transfer rate (fps)	9
Data transfer + power	USB

Table 1: Technical specification of the camera.

The used camera RIGI S2x is a new prototype that is optimized for low-frequency imaging. This is achieved through an optimized detector structure to enhance the absorption of low-frequency THz radiation.

Lens	
Focal length (mm)	44
f number	0.7
Lens material	HRFZ-Si
FoV (lateral \times vertical)	$17.3^\circ \times 13^\circ$
Operation range	7.4 – 3000 μm (0.1 – 30 THz)

Table 2: Technical specification of the lens.

2.2 Setups

A commercial THz-TDS system (Tera-FlashTF-1503 Ver. 4 Dec/2015, Toptica Photonics AG, Gräfelfing, Germany) was used as a starting point. In this system, a $100\ \mu\text{m}$ InGaAs based strip-line antenna serves as transmitter (TX). It is biased with 120 V and optically pumped by a pulsed 1550 nm Erbium fiber laser (pulse duration: 60 fs, repetition rate: 100 MHz). The 22.3 mW of NIR pump reaching the TX are converted to roughly $40\ \mu\text{W}$ cw equivalent, linearly polarized THz radiation. The THz-TDS scan time was kept fixed at 70 ps throughout all the experiments.

The optical setup is of the zigzag-transmission geometry type (see fig. 1): An OAPM collimates the diverging output of the TX, which is then focused by another OAPM. A sample can be placed in the beam waist. The transmitted radiation is guided by a second OAPM pair (rotationally symmetrical to the first one) onto the detector. In a standard THz-TDS, the detector would be a receiver (RX), working on the inverted principle of the TX. In this work, the RX was replaced with an uncooled microbolometer camera, which could be displaced along the THz propagation direction. Since the sensor is sensitive to all emitted wavelengths, the spectral resolution is not recoverable from the data. On the other hand, a high real-time spatial resolution is achieved, in contrast to the single-pixel nature of the RX. Furthermore, two wire-grid polarizers were inserted in the parallel beam sections to ensure a high degree of linear polarization. Additionally, they also allow for intensity reduction via the rotating polarizer method. To simplify the setup of figure 1, we removed all the OAPMs, illuminated the sample directly and captured the image with a lens specifically designed for the RIGI camera (fig. 2).

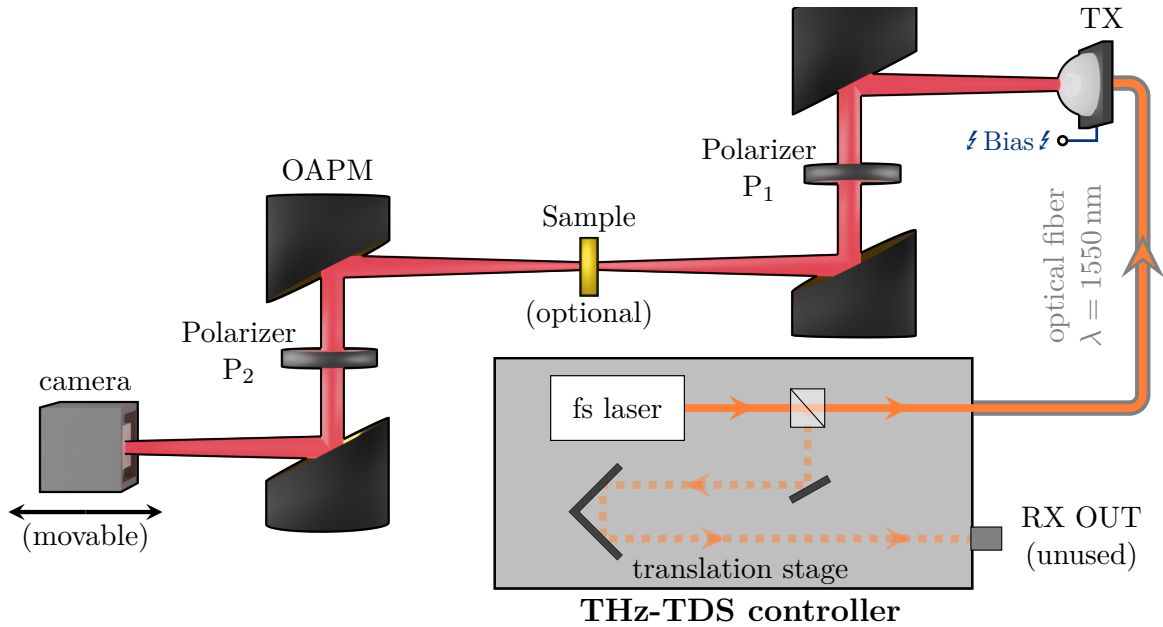


Figure 1: Schematic of the zigzag setup. Via an optical fiber, a fs pump laser ($\lambda = 1550\ \text{nm}$) excites the TX, which in turn emits THz radiation. Four OAPMs and two polarizers P_1, P_2 guide the THz emission onto the camera sensor (positioned where in a THz-TDS the RX would be located).

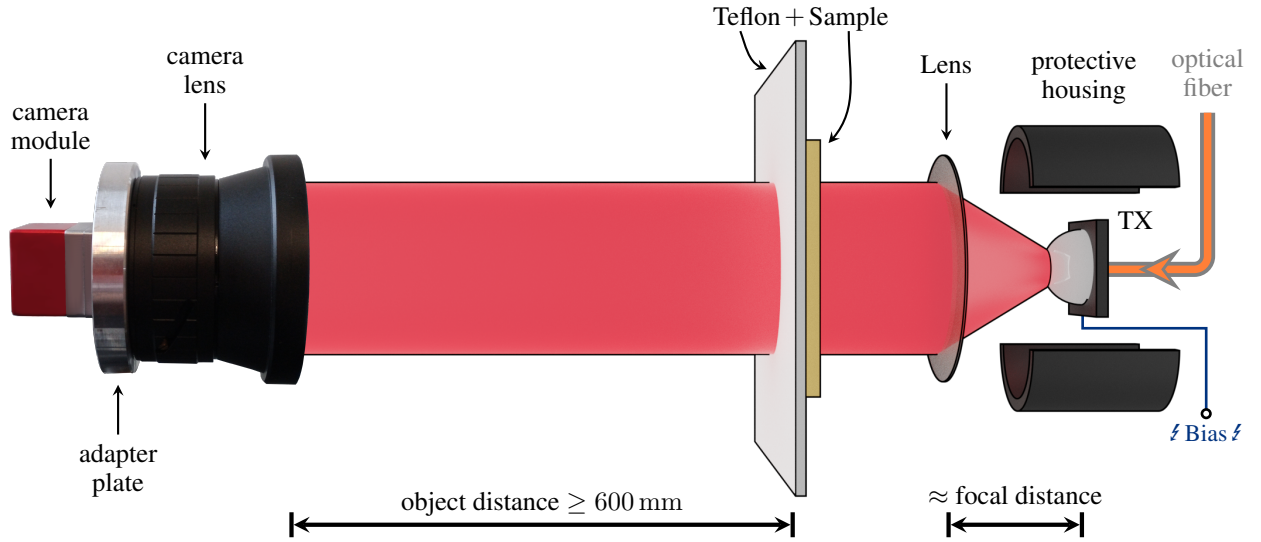


Figure 2: Schematic of the lens-based imaging setup. The THz emission of the TX is collimated by a silicon lens before it reaches the sample. To suppress the thermal image, the sample is mounted onto a sheet of Teflon. The transmitted radiation is recorded with the camera/lens combination placed more than 600 mm away from the object plane. Drawing not to scale.

For practical imaging applications, the complicated OAPM alignment is less favorable than the simpler lens-based setup depicted in figure 2. The TX is placed roughly in focus of a silicon (Si) lens ($f = 25$ mm, $d = 25$ mm), which collimates the divergent radiation of the THz emitter. The exact distance between lens and PCA determines the size of the illuminated area. The majority of the samples were mounted close to the collimating lens on a 1 mm thick sheet of Teflon for thermal image suppression. If this was not possible, a 3 mm Teflon sheet was placed between sample and camera. Furthermore, black polyethylene (PE) foil was fixed to the TX to weaken the leaking 1550 nm NIR pump pulses. Due to the design of the camera lens ($f = 44$ mm, f number = 0.7), the minimum object distance is 600 mm.

2.3 Image analysis and (post-)processing routines

The pre-processed image data from the camera was sent via USB to a PC. A control software allowed for real-time filtering and the saving of the data in different compressed and loss-less file formats. For this publication, the data were saved as 14 bit integer with minimal filtering into loss-less csv-files; only once compressed 8 bit jpg was used. In MATLAB, the following post-processing (also suitable for a real-time data stream) was applied: At first, dead pixels were removed by replacing them with a neighboring pixel. Optionally, images were then filtered with a 3×3 median filter followed by a Gaussian filter with a width of $\sigma = 1$ pixel. Then, a background image, captured while the THz beam was blocked and pre-processed with the same procedure, was subtracted. Afterwards, contrast enhancement was performed by re-scaling the minima/maxima of the gray-scale image data. For better visualization, some of the post-processed images were converted to false color.

Imaging of samples bigger than the illuminated area was made possible by scanning over the sample in real-time and stitching the single frames together. The position offset between the neighboring frames was determined by using auto-correlation in an area around the center of the image.

The spatial scaling of the THz images was estimated from the sensor pixel pitch and known feature dimensions measured on the samples. Sample (feature) dimensions were extracted with ImageJ/Fiji (see e. g. [38, 39]) from photographs of the samples on graph paper background.

3 Results

3.1 THz-TDS beam profiling

As a first proof-of-concept, the beam profile of the PCA emission was measured with the setup depicted in figure 1. In this configuration, we have a 1:1 imaging of the beam shape to the sensor. Since the intensity of the focused beam was too high for the extremely sensitive camera, the polarizer P_2 was rotated by $\theta \approx 65^\circ$, letting according to Malus's law ($I = I_0 \cdot \cos^2(\theta)$) [40] roughly 18% of the initial intensity pass. Assuming 50% further loss along the optical path, we expect an average intensity of less than 300 mW/m^2 at the detector, but we were still able to obtain decent contrast without any data processing (see figure 3 (a, b)).

The images in figure 3 represent single frames of a movie clip (see video S1 in supplementary materials), which was obtained by moving the camera along the THz propagation direction. Data acquisition was performed at 9 fps, allowing the experimenter to get immediate feedback. Even the unprocessed data directly streamed from the camera (fig. 3 (a, b)) provided sufficient information for a qualitative analysis. Post-processing the camera data (fig. 3 (c-f)) revealed that the beam out of focus (fig. 3 (c, f)) was elliptical and tilted about $\pm 45^\circ$ to the horizon. Close to the focus (fig. 3 (d, e)), the beam was slightly cross-shaped. Also, the continuous transition from $+45^\circ$ to -45° tilt could be resolved.

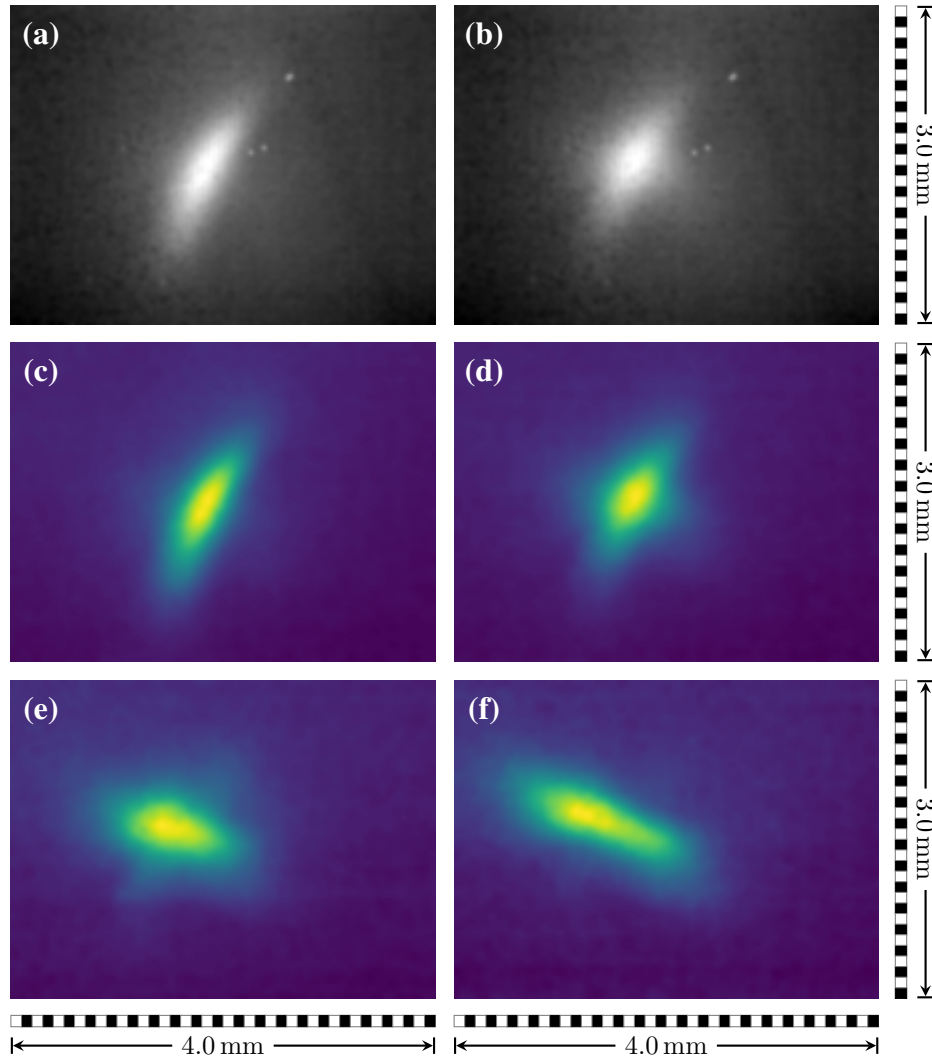


Figure 3: Selected single frames of a 1D real-time beam shape scan in propagation direction. Data as saved from camera software (a, b), and same data for comparison in false-color with post-processing applied (c, d). Subfigures (a, c, f) depict the beam shape for two out-of-focus positions (before/after focal point). The spatial intensity distribution close to optimal focus is presented in (b, d, e).

3.2 Siemens star

The first imaging tests were carried out on a Siemens star (photography with visible light (VIS) in fig. 4 (a), outer diameter $d = 12.5$ mm, rim diameter $d_{\text{rim}} = 10.6$ mm, 9 spokes), laser ablated from a thin metal sheet and mounted onto a 1 mm thick sheet of Teflon. To profit from the more intense sample irradiation in the THz-TDS (achievable intensity higher due to smaller beam size), the sample was placed into the standard position (see fig. 1). By intentionally shifting the first OAPM pair and TX closer to the sample, the focus is moved beyond the sample plane, effectively enlarging the illuminated sample area. With this approach, a part of the Siemens star could be imaged (fig. 4 (b)). However, the zigzag configuration with the OAPMs did not allow for an undistorted imaging of such a large sample. This was demonstrated by repositioning the Siemens star only slightly (fig. 4 (c)). Switching to the linear setup (fig. 2) allowed to resolve the complete Siemens star (fig. 4 (d)). For this data set, we did not use any spatial filtering to avoid its impact on the spatial resolution determination. Only dead pixel removal was applied (fig. 4 (e)). The recorded real-time video nicely shows the rotation of the Siemens star (see fig. 4 (f-h) and video S2 in supplementary materials), just with some minor intensity fluctuations and shifts.

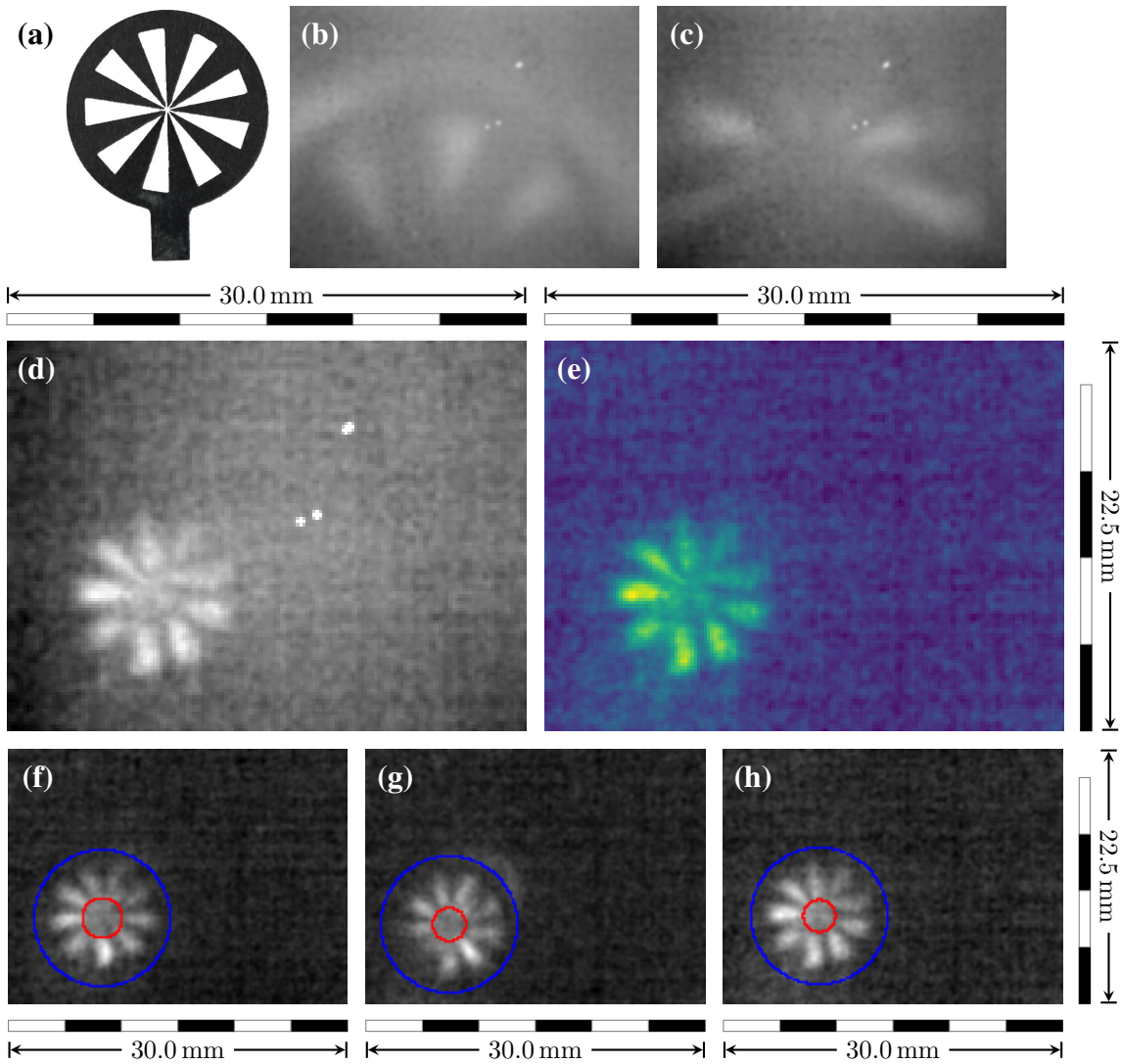


Figure 4: Imaging of a metallic Siemens star. Photography (VIS) of Siemens star (a). Unprocessed THz images acquired in zigzag THz-TDS geometry (see fig. 1): Image with outer rim of Siemens star visible (b), whereas in (c) only central part resolvable. THz images acquired in lens-based setup (see fig. 2): unprocessed THz data (d) and false-color with dead-pixel-removal applied (e). Determination of resolution shown with three example frames (f-h): Assumed outer rim of the Siemens star (blue circles) and resolution limit (red circles).

The quality of these images allow an estimation of the spatial resolution. First, the smallest radius r_{\min} of a centered circle is determined for which the average contrast between a spoke and an opening is larger than 10% of the highest contrast. The resolution is then $r_{\text{res}} = 2\pi \cdot r_{\min}/N$, where $N = 9$ is the number of spokes. For the current imaging setup a resolution $r_{\text{res}} = 1.05(15)$ mm was estimated from ten different Siemens star images.

3.3 Key in an envelope

We demonstrate the capability of our method for detecting concealed (metallic) objects from a larger distance by examining metallic keys (fig. 5 (a, d)), which were concealed with a standard paper envelope. Two very similar keys were placed into the THz beam approximately 600 mm away from the camera assembly (see fig. 2). The thermal image was suppressed with 3 mm of Teflon, located between sample and camera. As expected, a metal key without envelope was clearly resolved (fig. 5 (b)). The post-processing enhanced the contrast and made the edges more defined (fig. 5 (c), video S3 in supplementary materials). Putting a metal key into a paper envelope reduced the image quality due to absorption and diffraction on the rough paper surface (fig. 5 (e)). An additional quality loss originated from saving the data for testing purposes as 8 bit jpg, a format which seems not to be suitable for our THz imaging purposes. Overall, the key shape was fairly faint, but post-processing could enhance the visual clarity so far that even the edge of the paper envelope became visible (fig. 5 (f)). The video S4 in the supplementary materials shows how the experiment was performed in the laboratory.

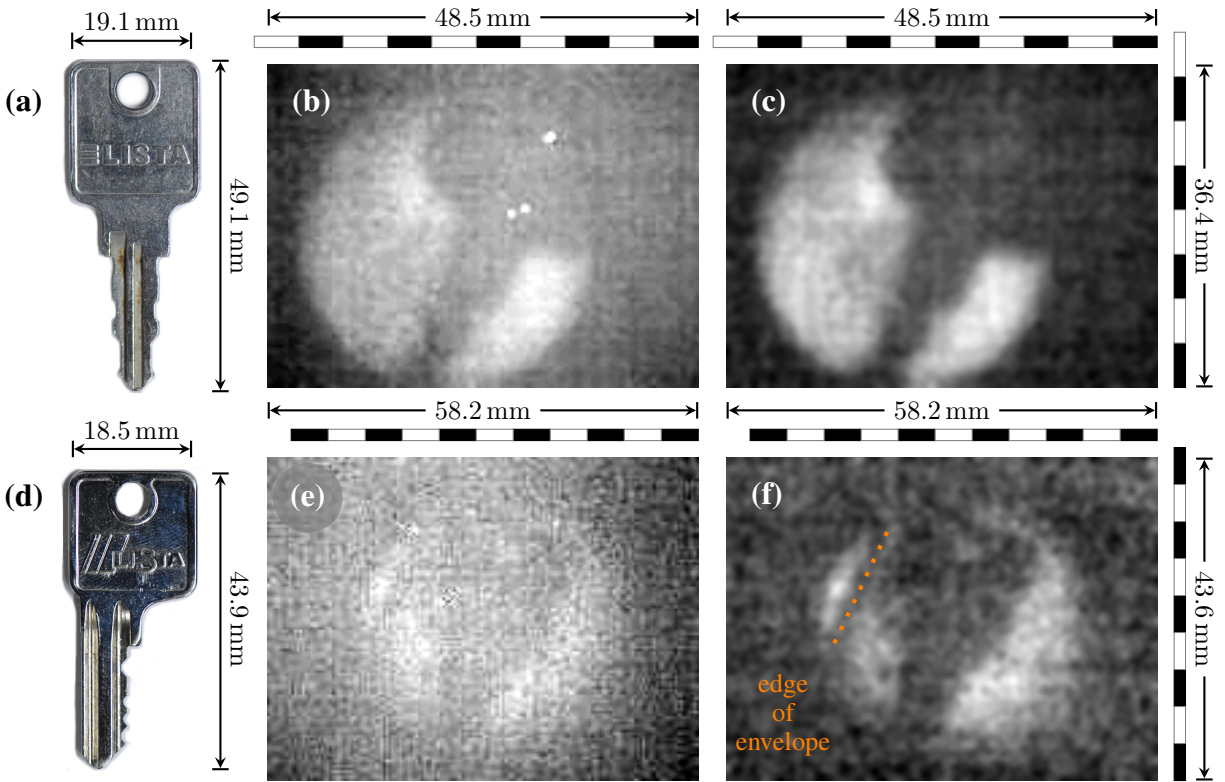


Figure 5: Imaging of metal keys. Photography of the keys with rough dimensions (a, d), raw THz images (b, e) of the keys, post-processed THz images (c, f) of the keys with dead pixel removal. A key can be still resolved within a standard paper envelope (e, f), with edge of envelope marked (f).

3.4 Leaves with different moisture contents

The strong absorption of water in the THz regime renders THz imaging an interesting modality for biological samples. We evaluated the potential of our approach by investigating leaves with different moisture contents. Three distinct leaf specimen (fig. 6 (a)) have been mounted on a 1 mm thick Teflon sheet and were scanned as described in subsection 2.3 and video S6 in supplementary materials. The stitched image (fig. 6 (b)) as well as exemplary single frames (fig. 6 (c-e) from video S5 in supplementary materials) provide the same distinct larger features like shape, cracks etc. as the photography (fig. 6 (a)). Additionally, the THz image shows leaves with higher moisture content distinctly darker. Although loosing the ability to resolve finer details, this could allow for an accurate qualitative analysis and even monitoring of diffusion processes in real-time.

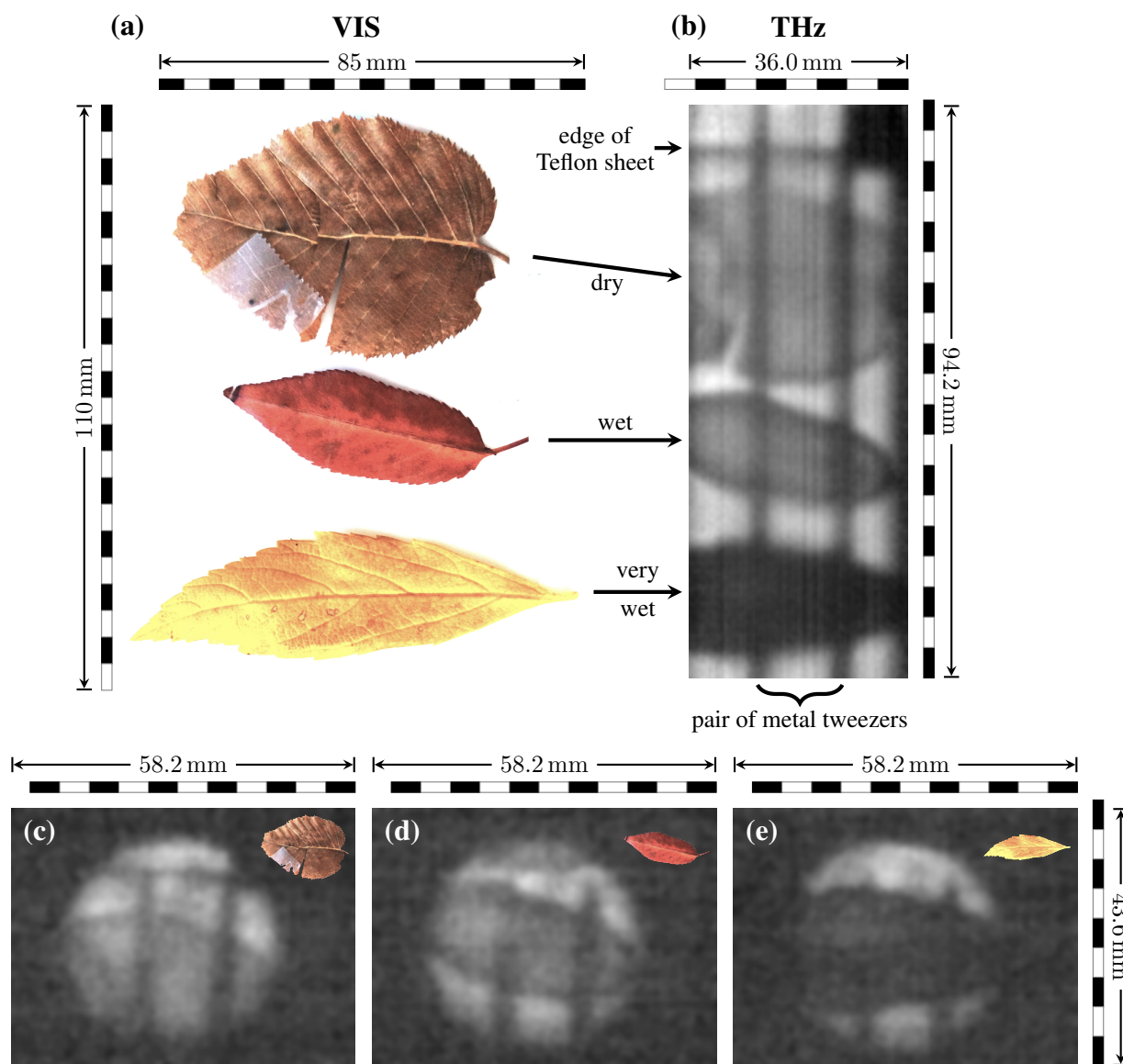


Figure 6: (a) Photography (VIS) of leaves with different water content. One leaf stored in drawer for five years (top), two picked up just before experiments: One from dry place (middle), one from wet gutter (bottom). Glued with THz transparent adhesive tape onto a 1 mm thick Teflon sheet; Teflon and tape stripes removed by image processing for better visual clarity; partially still visible. THz image of the different leaves (b) with a pair of tweezers for contrast enhancement (vertical lines) and the edge of the Teflon sheet (top, horizontal) visible. Higher water contents are clearly represented by decreased brightness. Image stitched with auto-correlation from single frames of a real-time 1D scan. An exemplary post-processed single frame is presented for the dry (c), wet (d) and very wet (e) leaf.

3.5 Thin wood sample

A 0.19 mm thin, microtome cut wood sample was mounted in a rotatable holder. Thermal image suppression was achieved with 3 mm of Teflon, located between sample and camera. The zero position of the rotation ($\varphi = 0^\circ$) was defined such that the annual rings were parallel to the polarization of the THz radiation. This preventive measure allows to determine whether any influence of the polarization on the recorded image exists.

An approximation for the illuminated area of the actual sample is shown for different orientations in the artistic illustration figure 7 (a). The annual rings are already visible in the raw THz images (fig. 7 (b)) and become more pronounced in the post-processed data (fig. 7 (c)). The annual rings are clearly recognizable for each configuration. There is no evidence that the ring orientation would influence the image contrast. The THz images (fig. 7 (b, c)) are single frames of a video clip (video S7 in supplementary materials) that we were able to record in real-time despite the high absorption.

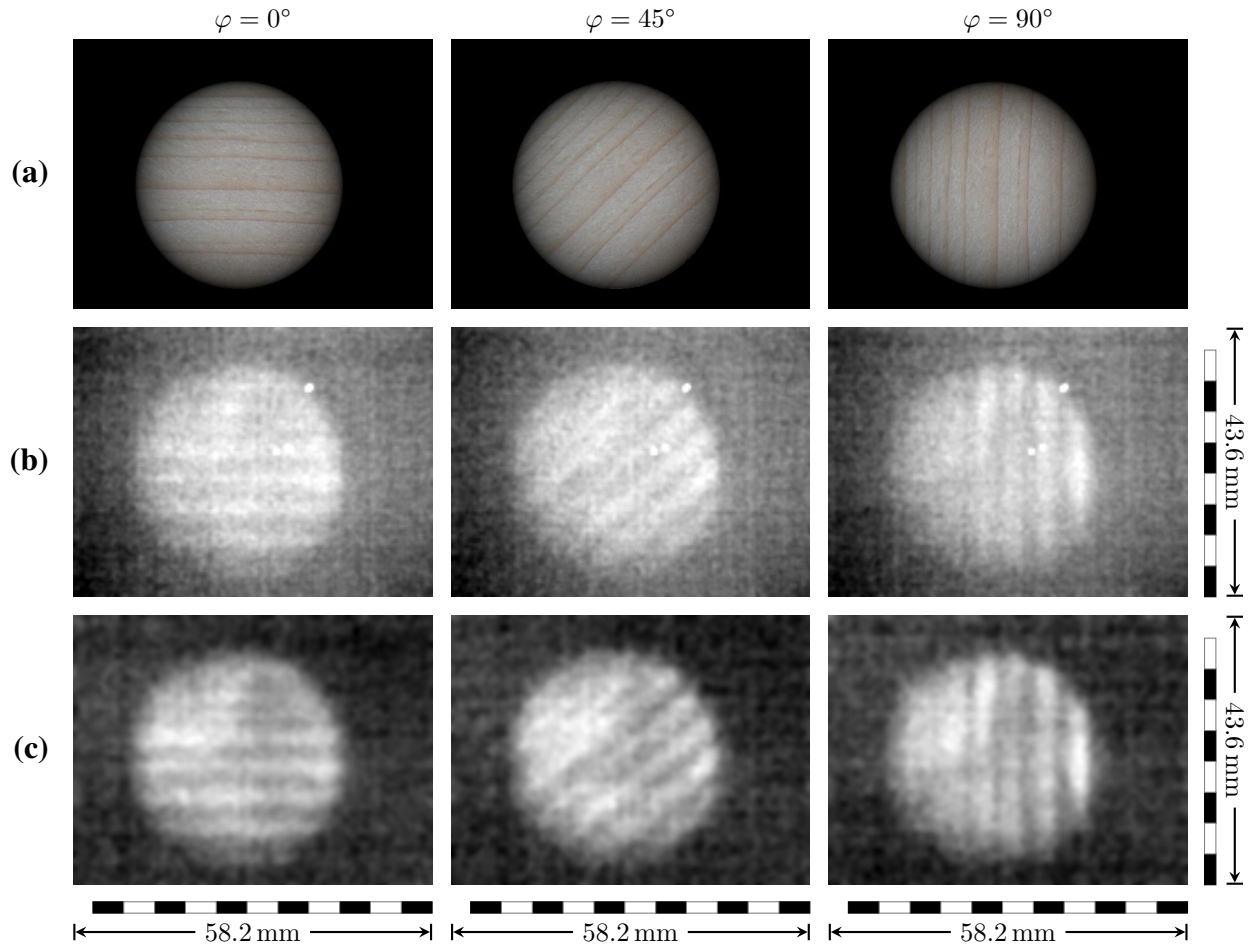


Figure 7: Imaging of a thin wood sample. (a) Not to scale artistic illustration of the approximate illumination of the thin wood sample for different angles φ , corresponding to the selected THz single frames from a full sample rotation recorded in real-time (b, c). Unprocessed data (b) as obtained from the camera and post-processed representation with dead pixel removal (c).

4 Discussion

4.1 Limitations and potential improvements of current setup

The major limitation of using a PCA as a THz source is the low output power. This is less relevant as long as images are acquired with a focused beam. However, for a collimated beam, the irradiance decreases quadratically with the beam radius. For example, a strong transmission signal through plastic (food) containers could be detected in the THz-TDS (focused, RX), but with the collimated beam and camera instead of RX, no valid signal could be recorded. Although the camera is extremely sensitive, the expanded beam combined with the sample absorption did not provide enough irradiance at the sensor for real-time imaging. For the current imaging setup, a resolution $r_{\text{res}} = 1.05(15)$ mm was estimated from the Siemens star images (fig. 4 (c-f)). This resolution is not far from the maximum we can expect if we compare it with the full width at half maximum of the smallest beam shape (fig. 3 (d, e)) of $0.65(10)$ mm and the wavelength of maximal intensity of the THz-TDS (0.6 mm corresponding to 0.5 THz), which determines the maximal achievable resolution. We presume that one relevant contribution to the limited resolution is the use of a broadband emitter instead of a single line source. Although the radiation contains high frequencies, which would allow for better spatial resolution, the dominant signal from lower frequencies blurs the image and dominates resolution properties. Furthermore, the strong water vapor absorption under ambient conditions greatly reduces the intensity of shorter wavelengths, leaving only longer wavelengths available for imaging. Since the image quality highly depends upon the optical path length, reducing the overall distance between source, sample and camera in conjunction with suppressing the water vapor influence would help. Not only if working over larger distances or under ambient conditions is absolutely required, the ongoing development of more efficient PCAs could provide a larger frequency bandwidth and higher intensities at shorter wavelengths. Blocking the lower frequencies with a high pass filter whilst still maintaining enough intensity for a high contrast THz image would allow resolving smaller structures which are not accessible with the current setup.

4.2 Potential applications

For the THz community, real-time beam profiling of weak and/or broad band sources like shown in figure 3 is still a difficult task. The results shown in this work also suggest that the new generation of very sensitive THz microbolometer cameras can image beams emitted from a PCA, but also other weak THz sources.

With the proof-of-concept that complex sample structures can be imaged (fig. 6 & fig. 7), the setup described in this work can also provide material scientists with easier access to THz experiments.

We can think of experiments with polymers, aerogels, (embedded) nanomaterials and materials derived from modified biological precursors. The latter class can also act as a bridge to biology. In-field, in-vivo experiments on leaves, grass, crops, young (tree) saplings are all within the realms of possibility. Due to the comparatively high portability, low power consumption and robustness, long term field experiments in remote locations without infrastructure/off-grid seem feasible.

From the capability to image biological samples, the agriculture and food industry could also profit directly, e. g. improving water management by monitoring the water content of leaves and plants. This has been demonstrated before with various THz setups [16]. Not only could this imaging method be applied during the production, but also ensure the product quality during transport and further processing, e. g. real-time detection of spoiled products or foreign bodies through packaging (see fig. 5). The latter one also immediately implies suitability for security applications like mail screening.

Further industrial use cases could be quality control during production, e. g. monitoring of the water content in paper, safety inspection or recycling of plastics, etc. Also thinkable would be THz photoelasticity, where one measures the stress states of THz-transparent materials in transmission.

The broad spectral range and polarization control can be used to visualize and evaluate residual stress distributions in packaging materials and electronic housings, but also to display stress distributions in real-time during a mechanical test.

4.3 Outlook: Possible modifications

Since imaging in the THz-TDS zigzag geometry has been shown (fig. 4 (b, c)), imaging using a PCA is not restricted to a conventional lens-based THz microscope. Instead of using lenses, setups with OAPMs specially designed for imaging are possible. This could allow accessing methods/samples which cannot be used/measured with commercially available (macro) lenses. A major disadvantage for achieving good image quality with this concept are the many degrees of freedom of an OAPM. This makes precise alignment very challenging, but exact calibration is an essential prerequisite for obtaining a high quality image.

During our initial experiments with the new source-detector combination, we focused on transmission. However, it is

straightforward to change the setup from transmission to reflection imaging by rearranging the illumination geometry. To mitigate the loss of time domain/spectral information caused by using a microbolometer camera instead of a conventional RX, we propose multi-spectral imaging via inserting THz band pass filters into the beam path. Mounting the filters onto a rotating wheel could allow the generation of false-color images in real-time. Its feasibility depends upon the quality of THz filters and the availability of PCA sources with higher power.

5 Conclusions

We presented a THz real-time imaging method based upon a fiber coupled PCA and an uncooled microbolometer camera. As a proof-of-concept, we recorded a THz-TDS beam shape in real time and examined the performance for typical security, quality control and material science tasks in transmission geometry. Challenges encountered during the experiment were the weak sample irradiance, a resolution lower than the physical wavelength limit and for some samples reduced image quality. Furthermore, we discussed possible improvements and (practical) applications of the setup, including experiments in reflection geometry and multi-spectral imaging with THz filters.

Supplementary Material

The following are available as supplementary material: Video S1: Real-time THz-TDS beam profiling, Video S2: Real-time rotation of metallic Siemens star, Video S3: Real-time THz imaging of a key, Video S4: Demonstration of laboratory equipment with concealed key, Video S5: Real-time moisture content resolution in leaves, Video S6: Demonstration of laboratory equipment with wet leaves, Video S7: Real-time rotation of thin wood sample.

Author contributions

Conceptualization, M. S. and P. Z.; RIGI imaging scheme prototype development: E. S.; Software, P. Z.; Validation, P. Z.; Formal Analysis, P. Z.; Investigation, M. S., P. Z.; Resources, M. S. and E. M.; Data Curation, P. Z.; Writing – Original Draft Preparation, E. H., P. Z., E. M. and M. S.; Writing – Review & Editing, E. H., P. Z., E. M. and M. S.; Visualization, P. Z.; Supervision, P. Z.; Project Administration, P. Z.

Funding

P. Z. gratefully acknowledges funding from the Swiss National Science Foundation, SNF project 200021_179061 / 1.

Acknowledgments

The authors would like to thank the following colleagues from Laboratory for Transport at Nanoscale Interfaces for their help: Jil Graf and Rolf Brönnimann, for the 3D printing and laser ablation, respectively, of some of the samples; Daniel Sacré: LaTeX support (typesetting, figure inclusion, layout), setup sketches and editing of videos in supplementary materials.

Additional thanks to Anselm Deninger, Toptica Photonics AG, Gräfelfing, Germany for providing insight into the property differences for PCAs of different generations.

Conflicts of interest

M. S. and E. S. declare to be affiliated with Swiss Terahertz GmbH, Park Innovaare, 5234 Villigen, Switzerland. Swiss Terahertz is the supplier of the RIGI camera and lens that were used in this work.

References

- [1] S. Wietzke, F. Rutz, C. Jördens, N. Krumbholz, N. Vieweg, C. Jansen, R. Wilk, and M. Koch. Applications of terahertz spectroscopy in the plastics industry. In Cunlin Zhang and Xi-Cheng Zhang, editors, *Photonics Asia 2007*, page 68400V, Beijing, China, 2007.
- [2] S. Wietzke, C. Jansen, N. Krumbholz, O. Peters, N. Vieweg, C. Jördens, M. Scheller, D. Romeike, T. Jung, M. Reuter, S. Chatterjee, M. Koch, Fachbereich Physik, B. Baudrit, T. Zentgraf, T. Hochrein, and M. Bastian. Terahertz spectroscopy: A powerful tool for the characterization of plastic materials. In *2010 10th IEEE International Conference on Solid Dielectrics*, pages 1–4, Potsdam, Germany, 2010. IEEE.

- [3] Andries Küter, Stefan Reible, Thomas Geibig, Dirk Nübler, and Nils Pohl. THz imaging for recycling of black plastics. *tm - Technisches Messen*, 85(3):191–201, 2018.
- [4] Mira Naftaly, Nico Vieweg, and Anselm Deninger. Industrial Applications of Terahertz Sensing: State of Play. *Sensors*, 19(19):4203, 2019.
- [5] Seiji Niijima, Masashi Shoyama, Kazumi Murakami, and Kodo Kawase. Evaluation of the sintering properties of pottery bodies using terahertz time-domain spectroscopy. *Journal of Asian Ceramic Societies*, 6(1):37–42, 2018.
- [6] Mikhail Mikerov, Rabi Shrestha, Peter van Dommelen, Daniel M. Mittleman, and Martin Koch. Analysis of ancient ceramics using terahertz imaging and photogrammetry. *Optics Express*, 28(15):22255, 2020.
- [7] Kodo Kawase, Adrian Dobroiu, Masatsugu Yamashita, Yoshiaki Sasaki, and Chiko Otani. Terahertz Rays to Detect Drugs of Abuse. In Robert E. Miles, Xi-Cheng Zhang, Heribert Eisele, and Arunas Krotkus, editors, *Terahertz Frequency Detection and Identification of Materials and Objects*, pages 241–250. Springer Netherlands, Dordrecht, 2007.
- [8] A. Giles Davies, Andrew D. Burnett, Wenhui Fan, Edmund H. Linfield, and John E. Cunningham. Terahertz spectroscopy of explosives and drugs. *Materials Today*, 11(3):18–26, 2008.
- [9] Wen-tao Liu, Jing-wen Li, and Wei Yang. Detection and identification of explosives and illicit drugs by terahertz spectroscopy technology. In *2010 IEEE International Geoscience and Remote Sensing Symposium*, pages 3576–3579, Honolulu, HI, USA, 2010. IEEE.
- [10] J. Meilhan, B. Dupont, V. Goudon, G. Lasfargues, J Lalanne Dera, D. T. Nguyen, J. L. Ouvrier-Buffer, S. Pocas, T. Maillou, O. Cathabard, S. Barbieri, and F. Simoens. Active THz imaging and explosive detection with uncooled antenna-coupled microbolometer arrays. In Mehdi Anwar, Nibir K. Dhar, and Thomas W. Crowe, editors, *SPIE Defense, Security, and Sensing*, page 80230E, Orlando, Florida, United States, 2011.
- [11] Tara M. Todoruk, Ian D. Hartley, and Matthew E. Reid. Origin of Birefringence in Wood at Terahertz Frequencies. *IEEE Transactions on Terahertz Science and Technology*, 2(1):123–130, 2012.
- [12] Soichi Tanaka, Keiichiro Shiraga, Yuichi Ogawa, Yoshihisa Fujii, and Shogo Okumura. Applicability of effective medium theory to wood density measurements using terahertz time-domain spectroscopy. *Journal of Wood Science*, 60(2):111–116, 2014.
- [13] Peter Zolliker, Markus Rüggeberg, Lorenzo Valzania, and Erwin Hack. Extracting Wood Properties From Structured THz Spectra: Birefringence and Water Content. *IEEE Transactions on Terahertz Science and Technology*, 7(6):722–731, 2017.
- [14] D. Banerjee, W. von Spiegel, M. D. Thomson, S. Schabel, and H. G. Roskos. Diagnosing water content in paper by terahertz radiation. *Optics Express*, 16(12):9060, 2008.
- [15] John F. Federici. Review of Moisture and Liquid Detection and Mapping using Terahertz Imaging. *Journal of Infrared, Millimeter, and Terahertz Waves*, 33(2):97–126, 2012.
- [16] Ralf Gente and Martin Koch. Monitoring leaf water content with THz and sub-THz waves. *Plant Methods*, 11(1):15, 2015.
- [17] Kiyong Jeong, Yong-Min Huh, Sang-Hoon Kim, Yeonji Park, Joo-Hiuk Son, Seung Jae Oh, and Jin-Suck Suh. Characterization of blood using terahertz waves. *Journal of Biomedical Optics*, 18(10):107008, 2013.
- [18] Maksim S. Kulya, Evgeniy L. Odlyanitskiy, Quentin Cassar, Ilia A. Mustafin, Valery N. Trukhin, Polina G. Gavrilova, Dmitry V. Korolev, Yulia A. Kononova, Nikolay S. Balbekin, Patrick Mounaix, Jean-Paul Guillet, Nikolay V. Petrov, and Olga A. Smolyanskaya. Fast Terahertz Spectroscopic Holographic Assessment of Optical Properties of Diabetic Blood Plasma. *Journal of Infrared, Millimeter, and Terahertz Waves*, 41(9):1041–1056, 2020.
- [19] Gombo Tzydynzhapov, Pavel Gusikhin, Viacheslav Muravev, Alexey Dremin, Yuri Nefyodov, and Igor Kukushkin. New Real-Time Sub-Terahertz Security Body Scanner. *International Journal of Infrared and Millimeter Waves*, page 10, 2020.
- [20] Erwin Hack, Lorenzo Valzania, Gregory Gäumann, Mostafa Shalaby, Christoph Hauri, and Peter Zolliker. Comparison of Thermal Detector Arrays for Off-Axis THz Holography and Real-Time THz Imaging. *Sensors*, 16(2):221, 2016.
- [21] Lorenzo Valzania, Yuchen Zhao, Lu Rong, Dayong Wang, Marc Georges, Erwin Hack, and Peter Zolliker. THz coherent lensless imaging. *Appl. Opt.*, 58(34):G256–G275, 2019.
- [22] A. Crocker, H. A. Gebbie, M. F. Kimmitt, and L. E. S. Mathias. Stimulated Emission in the Far Infra-Red. *Nature*, 201(4916):250–251, 1964.

- [23] L. Bosco, M. Franckić, G. Scalari, M. Beck, A. Wacker, and J. Faist. Thermoelectrically cooled THz quantum cascade laser operating up to 210 K. *Applied Physics Letters*, 115(1):010601, 2019.
- [24] Ali Khalatpour, Andrew K. Paulsen, Chris Deimert, Zbig R. Wasilewski, and Qing Hu. High-power portable terahertz laser systems. *Nature Photonics*, 15(1):16–20, 2021.
- [25] Markus Rösch, Giacomo Scalari, Mattias Beck, and Jérôme Faist. Octave-spanning semiconductor laser. *Nature Photonics*, 9(1):42–47, 2015.
- [26] Kazuue Fujita, Seungyong Jung, Yifan Jiang, Jae Hyun Kim, Atsushi Nakanishi, Akio Ito, Masahiro Hitaka, Tadataka Edamura, and Mikhail A. Belkin. Recent progress in terahertz difference-frequency quantum cascade laser sources. *Nanophotonics*, 7(11):1795–1817, 2018.
- [27] Yuan Jin, John L. Reno, and Sushil Kumar. Phase-locked terahertz plasmonic laser array with 2 W output power in a single spectral mode. *Optica*, 7(6):708–715, 2020.
- [28] Roman J.B. Dietz, Björn Globisch, Helmut Roehle, Dennis Stanze, Thorsten Göbel, and Martin Schell. Influence and adjustment of carrier lifetimes in InGaAs/InAlAs photoconductive pulsed terahertz detectors: 6 THz bandwidth and 90dB dynamic range. *Optics Express*, 22(16):19411, 2014.
- [29] Martin van Exter, Ch Fattinger, and D. Grischkowsky. Terahertz time-domain spectroscopy of water vapor. *Opt. Lett.*, 14(20):1128–1130, 1989.
- [30] K. Krügener, S.F. Busch, A. Soltani, M. Schwerdtfeger, E. Castro-Camus, M. Koch, and W. Viol. THz time domain spectroscopy — Non-destructive evaluation of material detachments from exposed natural stone and ceramic objects. In *2017 42nd International Conference on Infrared, Millimeter, and Terahertz Waves (IRMMW-THz)*, pages 1–2, Cancun, Mexico, 2017. IEEE.
- [31] K. Krügener, J. Ornik, M. Schneider, A. Jackel, E. Castro-Camus, M. Koch, and W. Viol. On-site inspection of conservation works using THz TDS. In *2019 44th International Conference on Infrared, Millimeter, and Terahertz Waves (IRMMW-THz)*, pages 1–2, Paris, France, 2019. IEEE.
- [32] Kirsti Krügener, Jan Ornik, Lorentz M. Schneider, Alexander Jäckel, Corinna L. Koch-Dandolo, Enrique Castro-Camus, Nicole Riedl-Siedow, Martin Koch, and Wolfgang Viöl. Terahertz Inspection of Buildings and Architectural Art. *Applied Sciences*, 10(15):5166, 2020.
- [33] K. Fukunaga, Hosako, I., Kohdzuma, Y., Koezuka, T., Kim, M.-J., Ikari, T., and Du, X. Terahertz analysis of an East Asian historical mural painting. *Journal of the European Optical Society - Rapid publications*, 5:4, 2010.
- [34] J. Bianca Jackson, Julien Labaune, Rozenn Bailleul-Lesuer, Laura D’Alessandro, Alison Whyte, John W. Bowen, Michel Menu, and Gerard Mourou. Terahertz pulse imaging in archaeology. *Frontiers of Optoelectronics*, 8(1):81–92, 2015.
- [35] X. Li and M. Jarrahi. A 63-Pixel Plasmonic Photoconductive Terahertz Focal-Plane Array. In *2020 IEEE/MTT-S International Microwave Symposium (IMS)*, pages 91–94, 2020.
- [36] Helmut Fischer GmbH. Non-destructive measurements with terahertz radiation. *IST International Surface Technology*, 11(1):58–59, 2018.
- [37] Rayko Ivanov Stantchev, Xiao Yu, Thierry Blu, and Emma Pickwell-MacPherson. Real-time terahertz imaging with a single-pixel detector. *Nature Communications*, 11(1):2535, 2020.
- [38] Caroline A Schneider, Wayne S Rasband, and Kevin W Eliceiri. NIH Image to ImageJ: 25 years of image analysis. *Nature Methods*, 9(7):671–675, 2012.
- [39] Johannes Schindelin, Ignacio Arganda-Carreras, Erwin Frise, Verena Kaynig, Mark Longair, Tobias Pietzsch, Stephan Preibisch, Curtis Rueden, Stephan Saalfeld, Benjamin Schmid, Jean-Yves Tinevez, Daniel James White, Volker Hartenstein, Kevin Eliceiri, Pavel Tomancak, and Albert Cardona. Fiji: An open-source platform for biological-image analysis. *Nature Methods*, 9(7):676–682, 2012.
- [40] Heinz Niedrig, editor. *Optik*, volume 3 of *Bergmann - Schäfer: Lehrbuch Der Experimentalphysik*. Walter de Gruyter, Berlin, New York, tenth edition, 2004.